NJC

New Journal of Chemistry

A journal for new directions in chemistry

Accepted Manuscript

This article can be cited before page numbers have been issued, to do this please use: H. Liu, T. Yan, Z. Jin and Q. Ma, *New J. Chem.*, 2020, DOI: 10.1039/C9NJ05977F.

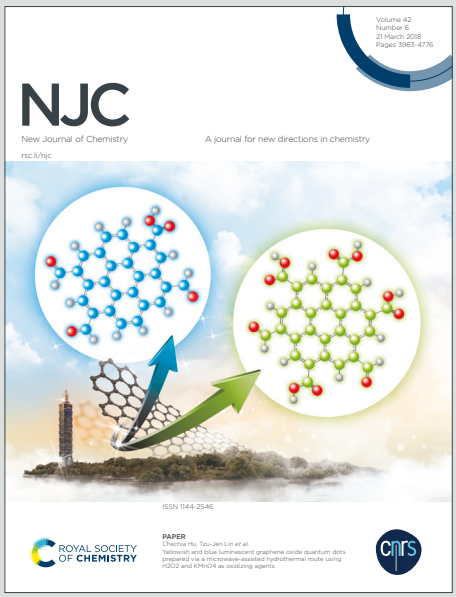

This is an Accepted Manuscript, which has been through the Royal Society of Chemistry peer review process and has been accepted for publication.

Accepted Manuscripts are published online shortly after acceptance, before technical editing, formatting and proof reading. Using this free service, authors can make their results available to the community, in citable form, before we publish the edited article. We will replace this Accepted Manuscript with the edited and formatted Advance Article as soon as it is available.

You can find more information about Accepted Manuscripts in the Information for Authors.

Please note that technical editing may introduce minor changes to the text and/or graphics, which may alter content. The journal's standard Terms & Conditions and the Ethical guidelines still apply. In no event shall the Royal Society of Chemistry be held responsible for any errors or omissions in this Accepted Manuscript or any consequences arising from the use of any information it contains.

DOI: 10.1039/C9NJ05977F

CoP nanoparticles as cocatalyst modified the CdS/$NiWO_4$ of p-n heterojunction to produce hydrogen efficiently

Hua Liu [1,3,4], Teng Yan[1,3,4], Zhiliang Jin[1,2,3,4*], Qingxiang Ma[2*]

1. School of Chemistry and Chemical Engineering, North Minzu University, Yinchuan 750021, P.R.China

2. State Key Laboratory of High-efficiency Utilization of Coal and Green Chemical Engineering, Ningxia University, Yinchuan,750021, PR China

3. Ningxia Key Laboratory of Solar Chemical Conversion Technology, North Minzu University, Yinchuan 750021, P.R.China

4. Key Laboratory for Chemical Engineering and Technology, State Ethnic Affairs Commission, North Minzu University, Yinchuan 750021, P.R.China

Corresponding author: zl-jin@nun.edu.cn (Z. L. Jin); maqx@nxu.edu.cn (Q. X. Ma)

Abstract: Generally, co-catalyst modification is an efficient way to enhance the hydrogen evolution performance of visible light irradiation. In this work, CoP nanoparticles act co-catalyst to modify the CdS/$NiWO_4$ p-n heterojunction. The composite catalyst CdS/$NiWO_4$/CoP was successfully prepared by co-precipitation and physical mixing method. The maximum H_2 production rate of composite catalyst is 47.7 mmol h^{-1} g^{-1}, which are 11.9 times and 3.3 times that of pure CdS and CdS/$NiWO_4$ (50%wt), respectively, and the apparent quantum efficiency is 9.7% in the 10% lactic acid system when the wavelength is 475 nm. This excellent performance is attributed to CoP nanoparticles, which act as electron traps to provide more active sites and benefit electron transport. The photoluminescence spectroscopy and electrochemical performance analysis demonstrated that the composite catalyst has better electron separation ability and light absorption conversion ability. The Mott-Schottky and UV-visible diffuse reflectance testing indicated that the excellent electron and holes separation was due to the p-n junction formed between CdS and $NiWO_4$, and the modification of CoP co-catalyst further enhanced the charge separation efficiency, thereby improving hydrogen evolution activity.

Key words: cocatalyst, CoP nanoparticles, hydrogen evolution, charge separation.

1. Introduction

The development of society cannot be separated from the use of fossil fuels. Nowadays, fossil fuels are not only shortage, but also cause a series of serious environmental pollution problems [1-3]. The solar energy and hydrogen energy make great concern to scientists as clean and renewable energy [4-6]. Photocatalytic hydrogen production which is considered to be one of the effective ways to solve the current problems can make good use of solar energy as well as produce hydrogen [7]. Platinum has been widely used as catalyst for photocatalytic hydrogen production, however, its high cost limit its further development [8]. Finding for cheap and efficient catalysts instead of platinum is great significance for promoting photocatalytic hydrogen production to fulfill large-scale industrial production [9-11].

Over the past few decades, many non-precious metal catalysts have been studied, such as carbon-based materials [13, 14], transition metal oxides [15, 16], metal sulfide [17, 18], hydroxides [19] and so on. Among of these catalyst, metal sulfide have narrow band gap and strong absorption ability of visible light, such as CdS [20-22], $ZnIn_2S_4$ [23], and CdZnS [24]. Especially CdS is used to enhance the absorption of visible light and crack water due to its appropriate band gap (about 2.4 eV) as well as used to improve the edge potential due to its appropriate conduction band [25, 26]. Unfortunately, the H_2 production activity of pure CdS is not ideal due to the rapid recombination of photocarrier and the easy occurrence of photocorrosion [27]. The performance of CdS used as catalyst was improved by morphology regulation, element doping, catalyst modification and heterogeneous junction construction [28, 29].

It is a common method to improve hydrogen production efficiency by loading co-catalyst on catalyst surface [30]. The main functions of the co-catalyst include: effectively promoting the separation of photogenic carriers; Reduce the semiconductor over potential or activation energy to enhance the reduction ability of the catalyst [31]. Transition metal phosphide is a common co-catalyst with low over potential, good stability and friendly to the environmental. Especially，the stability of CoP in acid-based media is comparable to that of zero-valence metal [32]. In the aspect of hydrogen production, the research on transition metal phosphates as a cocatalyst began around 2014 [33]. Tian et al. [34] prepared CoP/WS_2 by combination of vulcanized and phosphatize, they proved that CoP is an efficient catalyst for hydrogen production. Du's group [35] reported that by attaching Ni_2P to the surface of in situ, hydrogen production performance can be

significantly improved. Wang et al. [36] confirmed the hydrogen production efficiency while using lamellar $Ni_2P/g\text{-}C_3N_4$ as catalyst is 22 times than use pure $g\text{-}C_3N_4$. However, there are very few reports concerned the CoP nanoparticles as catalyst to modify heterojunction.

In this article, $CdS/NiWO_4/CoP$ composite catalyst was successfully prepared according to the follow steps. First, the $NiWO_4$ loaded on CdS by the co-precipitation, from the p-n heterojunction $CdS/NiWO_4$. Second, the CoP nanoparticles are used as catalyst to modify the $CdS/NiWO_4$ p-n heterojunction by the physical mixing. The successful preparation of ternary composites material $CdS/NiWO_4/CoP$ has significantly increased hydrogen production activity and light absorption property. The CSNP-7 ternary composites improved photo catalytic H_2 conversion rate to 47.7 mmol h^{-1} g^{-1} which are 11.9 and 3.3 times higher than that of CSNW-5 and bare CdS, respectively. This excellent performance is attributed to the modification of CoP nanoparticles, acting as electron traps to provide more active sites and benefit electron transport and improving the photo absorption ability of catalyst. This report provides a new research idea for the decomposition of water into hydrogen by multi-component catalysts.

2. Experimental Section

All reagents are with analytical grade and used without more settlement.

2.1 Preparation of CdS nanorods, $CdS/NiWO_4$ and CoP nanoparticles

The preparation of CdS nanorods: 2 g of $C_4H_6CdO_4{\cdot}2H_2O$ and 1.75 g of H_2NCSNH_2 were equably dispersed in 50 mL of ethylenediamine with uniform stirring for 1 h. Subsequently, the above solution was added into 80 mL Teflon-lined, then the autoclave was sealed and reacted carried out at 160 °C for 24 h. After that, the mixtures was centrifuged and washed with deionized water and ethanol, respectively. The final CdS was obtained by drying at 60 °C for 8 h.

The preparation of $CdS/NiWO_4$ (CSNW): The composite catalyst CSNW was synthesized by the co-precipitation [37]. Taking the preparation of CSNW-5 ($m(NiWO_4)/m(CdS)\times100\%=50$, named as CSNW-5) as an example. First, 0.2 g of CdS was added in 60 mL of deionized water by ultrasound for 10 min, and then 0.077 g $NiCl_2{\cdot}6H_2O$ and 0.107 g $Na_2WO_4{\cdot}6H_2O$ were added to above the solution. After stirring for 2 h, the compound was centrifuged and washed with deionized water and alcohol, respectively. The CSNW was obtained by drying at 60 °C for 10 h. CSNW-2, CSNW-3, CSNW-4 and CSNW-6 were prepared by the same method. The synthesis

View Article Online
DOI: 10.1039/C9NJ05977F

process of pure $NiWO_4$ was similar without CdS under the same method.

2.2 Preparation of CoP nanoparticles, CdS/$NiWO_4$/CoP and CdS/CoP.

The preparation of CoP nanoparticles: 1 g of $Co(NO_3)_2 \cdot 6H_2O$ and 0.25 g sodium citrate were dispersed in 35 mL of deionized water. Then, 10 mL (7 M) NaOH solution was tardily added and stirred at room temperature for 1 h. After centrifugation, they were washed three times with deionized water and alcohol, respectively. The reaction precursor was obtained by drying in an oven at 60 °C overnight. 1 g of reaction precursor was dissolved in 20 mL of H_2O with 2 g of $NaPO_2H_2 \cdot H_2O$. The mixture was ground to a powder after evaporation. It was calcined with N_2 at 300 °C for 4 h. Composite was obtained after centrifuge drying. 0.1 g of composite was steeped in 30 mL (3 M) HCl for 30 min, CoP nanoparticles were grinded after centrifuge drying.

The preparation of CdS/$NiWO_4$/CoP (CSNP): CSNP were compounded by the physical mixing. Taking the preparation of CSNP-5 (m(CoP)/m(CSNW)×100%=5, named as CSNP-5) as an example. As prepared 0.5 g of CSNW and 0.025 g of CoP nanoparticles were added to the 30 mL anhydrous ethanol with ultrasound for 20 min to form a homogeneous solution. The ethyl alcohol was evaporated at 80 °C and the last dried at 60 °C. It was simply labeled CSNP-5. The CSNP-1, CSNP-3, CSNP-7 and CSNP-9 were prepared in the same way.

The preparation method of CdS/CoP (CSCP): CSNP were compounded by the physical mixing. First, 0.5 of pure CdS and 0.35 g of CoP nanoparticles were dispersed in 30 mL anhydrous ethanol by ultrasound for 20 min. The uniformly stirring for 2 h to homogeneous solution, then steam dry at 60 °C water bath. The CSCP was obtained by drying at 60 °C for 10 h, It was simply labeled CSCP-7.

2.3 Characterization of samples

All kinds of morphology and structure of CdS, CSNW and CSNP were detected by taking the scanning electron microscope (SEM: Hitachi S-4800) with an accelerating voltage of 5.0 kV and a transmission electron microscopy (TEM: Tecnai G2-TF30), energy dispersive X-ray (EDX) under the acceleration voltage of 300 kV. The crystalline structure was analyzed by X-ray diffraction (XRD: Rigaku RINT-2000) patterns. X-ray photoelectron (XPS: ESCALAB 250Xi) was introduced to record the element composition. UV-vis DRS was obtained by UV-2550 (shimazu) spectrometer with using $BaSO_4$ as a reference. The ASAP2020M instrument was employed measure the adsorption-desorption isotherms of nitrogen by analyzing the result with the

Brunaure-Emmett-Teller (BET) equation. The FlUOROMAX-4 spectrophotometer (HORIBA Scientific, France) was engage to test photoluminescence (PL) emission and time-resolved spectra. An electrochemical workstation (VersaSTA4-400, AMETEK) is used to detection the photoelectrochemistry quizzes containing photocurrent density-time (I-T), electrochemical impedance spectrum (EIS) and Mott-Schottky measurements, there into 0.2 mol/L Na_2SO_4 aqueous solution as a electrolyte. The standard three-electrode cell consisted of Pt sheet as the counter electrode, the reference electrode is saturated calomel electrode (SCE), and homemade surface of work electrodes was 1 cm^2. Furthermore, the test of I-T curve is performed in the light source is 300 W xenon lamp cases at a fixed bias of 0.3 V vs. SCE. When the forward bias is 0.2 V, the samples of EIS are measured are measure at AC amplitude of 10 mV and a frequency scope is 10000-1 Hz. Meanwhile, the AC amplitude of 10 mV, the Mott-Schottky of CdS and $NiWO_4$ is tested from -1 to 1 Vs with at a frequency of 1000 HZ.

2.4 Photocatalytic H_2 measurements

Photocatalytic hydrogen production activity of all as-prepared samples is carried out in a 62 mL reaction bottle. First, the 0.01 g ternary composite catalysts were uniformly dispersed by ultrasound in 30 mL of 10% lactic acid solution. N_2 was purged into the reaction bottle 10 min to keep the reaction system in an anaerobic atmosphere by filling the N_2 about 10 min to replace O_2. The gas chromatography (Tianmei GC7900, TCD, 13X column, N_2 as the carrier) system was used to analyze extract 0.5 mL of H_2 evolved every one hour. In addition, stability experiments are also carried out at room temperature and each cycle of 5 h each, the total amount of hydrogen produced is calculate by the external standard method.

Further, the apparent quantum efficiency (AQE) of the CSNP-7 was tested out using xenon lamps at 300 W. The PL-MW200 radiometer (Perfect Light) was used to test photon fluxes before and after illumination. The experimental condition was basically the same as the hydrogen production procedure except for the light source. The monochromatic wavelength is 420, 450, 475, 500, 520 and 550 nm. Calculating the apparent quantum efficiencies by Eq (1) at different wavelengths

$$AQE = \frac{2 \times the\ number\ of\ evolved\ hydrogen\ molecules}{the\ number\ of\ incident\ photon} \times 100\% \quad (1)$$

3. Results and discussion

3.1 XRD analysis

Fig. 1 shows the X-ray diffraction patterns of bare CdS, $NiWO_4$, CoP, CSNW and CSNP composites with different ratios. In **Fig. 1A**, seven distinct characteristic diffraction peaks at 24.9°, 26.6°, 28.3°, 43.7°, 47.9°, and 51.9° can be assigned to the (100), (002), (101), (102), (110), (103) and (112) crystal plane of CdS (PDF#41-1049), respectively [6, 18]. However, the XRD patterns of CSNW-5 have not discovered corresponding peak of $NiWO_4$, which is probably because $NiWO_4$ is amorphous. In **Fig. 1B**, CoP has five characteristic peaks of 30.1°, 30.5°, 32.5°, 33.6° and 36.8° corresponding to (011), (111), (112), (211) and (301) crystal plane of CoP (PDF#89-4862) [8], which prove the successful preparation of CoP. Nevertheless, no obvious CoP characteristic diffraction peaks in the CSNP-7 composite catalyst, which may because content of CoP is relatively low. As shown in **Fig. 1C**, pure NiWO4 has two scattered and widened peaks located at 30.88°, 54.71° can be indexed to $NiWO_4$ (PDF#72-480), may be caused by amorphous $NiWO_4$.

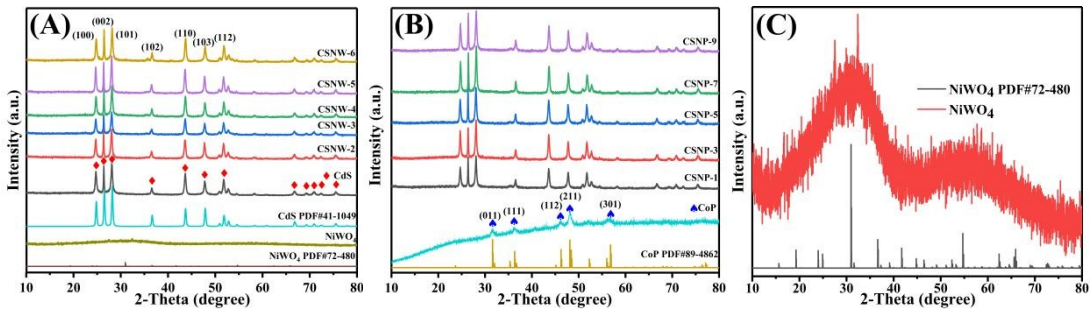

Fig. 1 XRD patterns of **(A)** Pure CdS, $NiWO_4$ and different proportions of CSNW, **(B)** CoP and CSNP composites with different CoP content, **(C)** $NiWO_4$ samples.

3.2 SEM and TEM analysis

The morphology of CdS and CSNP-7 samples are investigated by SEM and TEM, which are utilized to offer more intuitive information about the sample distribution, size and space shape of samples and so on. The bar shape CdS with smooth surface has a very uniform shape size in **Fig. 2A**. As depicted in **Fig. 2B**, the composite catalyst CSNP-7 has coarser surface compared with that of the pure CdS nanorods, the aggregation state of $NiWO_4$ is close contact with CdS nanorods, at the same time, ultra small of CoP nanoparticles are equably loaded on the surface of CdS and $NiWO_4$, this spatial distribution of CoP nanoparticles can expose more active sites, immensely

improving the hydrogen production performance of composite catalyst. Fig. 2C shows the EDX spectrum of the CSNP-7 which demonstrate the existence of Cd, S, Ni, W, O, Co and P elements, so the successful preparation of CSNP-7 may be proved. Further, Cu element is detected in the spectrums, which principally come from Cu carriers [40]. In **Fig. 2 D**, CdS nanorods has sloppy surface and the size is about the same, which is in agreement with the SEM consequence. It can be seen from **Fig. 2F** that the outer surface of CSNP-7 becomes rough the when the CoP and $NiWO_4$ were loaded on the surface of CdS nanorods, which proves that $NiWO_4$ and CoP are successfully loaded on the surface of CdS nanorods. More importantly, there are a lot of tiny CoP nanoparticles loaded on the surface of CSNW-5. As observed in **Fig. 2E**, the lattice fringes of the composite catalyst CSNF-7 are obviously observe by high resolution transmission electron microscopy (HRTEM), which it can be seen that the lattice fringe spacing of 0.336 nm and 0.247 nm are corresponded to the (002) planes of CdS (PDF#41-1049) and (111) planes of CoP (PDF#89-4862). Simultaneously, lattice fringes of $NiWO_4$ are absent, once again shows that $NiWO_4$ is amorphous, which is in agreement with the XRD results. In the next place, the $NiWO_4$ covers the lattice fringes of CdS, which proves the $NiWO_4$ exists on the surface of CdS in a deposited manner. **Fig. 2G** and **2H** shows the TEM images of the CSNP-7 samples obtained after the recycled tests. It can be easily found that the fresh CSNP-7 and recycled CSNP-7 samples have the same lattice fringes, indicating the compound catalyst has reusability and excellent stability.

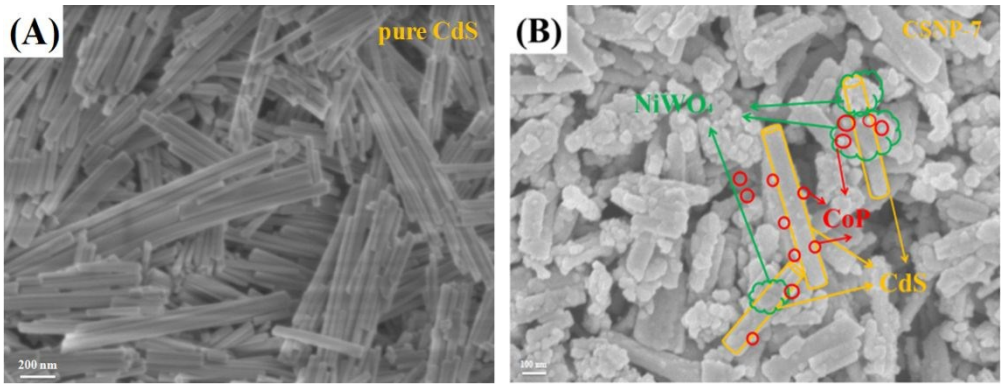

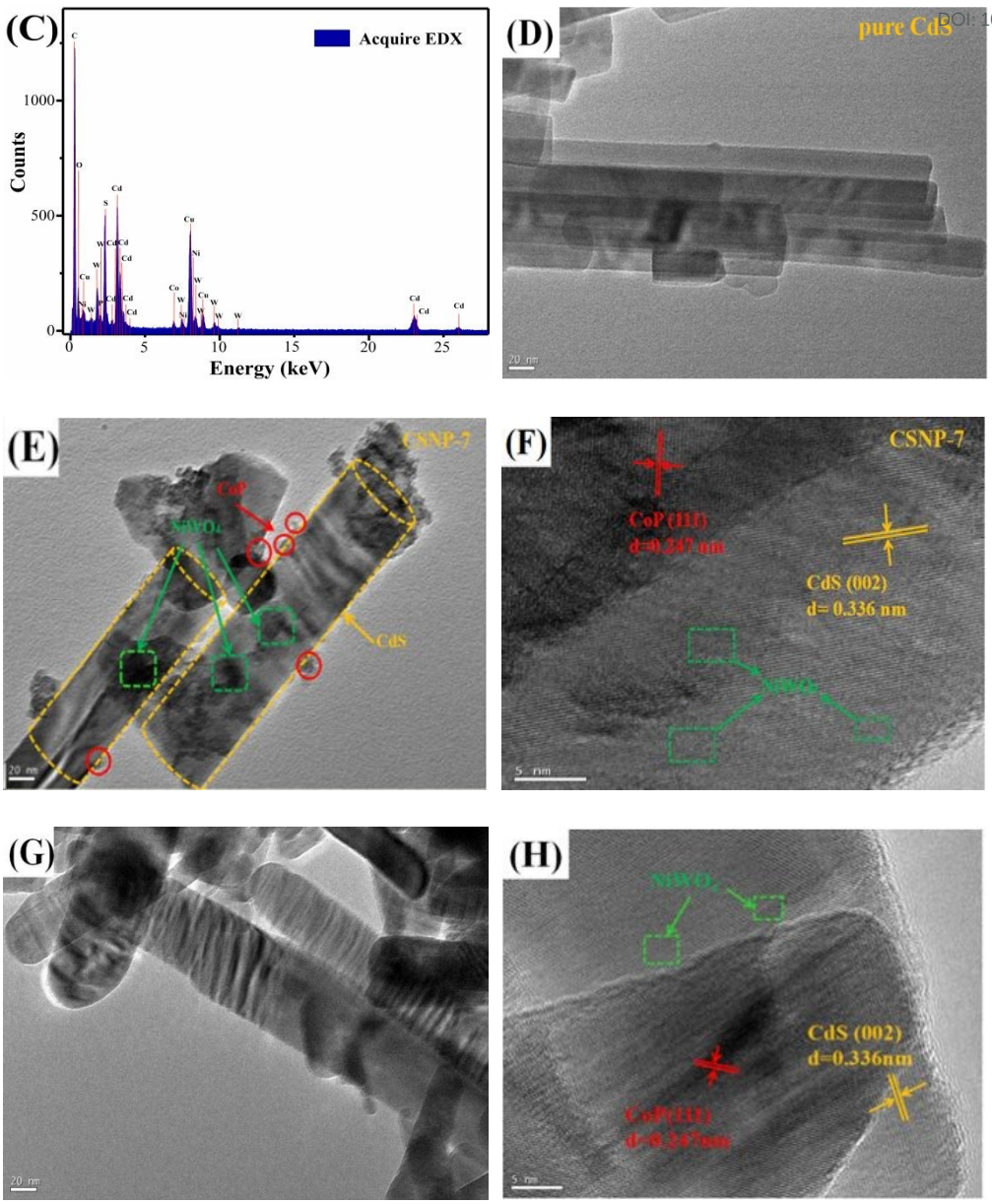

Fig. 2 (A) SEM images of pure CdS and **(B)** CSNP-7; **(C)** the EDX spectrum of CSNP-7; TEM images (D) pure CdS ; **(E)** TEM images of CSNP-7 and **(F)** HR-TEM images of CSNP-7; TEM images after cyclic stability tests for **(G)** CSNP-7 and **(H)** HR-TEM images of CSNP-7.

3.3 XPS analysis

The valence state and chemical composition of CSNP-7 samples before and after hydrogen production are investigated by X-ray photoelectron spectra (XPS) as in **Fig. 3**. **Fig. 3A** represents the XPS spectra of Cd 3d, S 2p, Ni 2p, W 4f, O 1s, Co 2p and P 2p for CSNP-7, and the peaks corresponding to the elemental composition are in good agreement with the reported literature [10, 21, 39, 40, 41, 42]. **Fig. 3B** shows that the peaks of Cd 3d located at 405.1 and 411.8 eV, which are belong to Cd $3d_{5/2}$ and Cd $3d_{3/2}$ respectively for Cd^{2+} state. As shown in **Fig. 3C,** along with

the peaks of S 2p are observed at 161.5 and 162.7 eV, belonging to S $2p_{3/2}$ and S $2p_{1/2}$ of S^{2-} [21]. **Fig. 3D** shows the Ni $2p_{3/2}$ and Ni $2p_{1/2}$ binding energies are noted at 855.8 and 873.5 eV, respectively, together with satellite peaks assured at 862.0 and 879.4 eV. The distance in binding energy (17.7 eV) between the two peaks of Ni $2p_{1/2}$ and Ni $2p_{3/2}$ verifier the divalent oxidation state of Ni atoms exist in $NiWO_4$ nanostructures [10, 39]. As shown in **Fig. 3E** and **3F**, the W 4f spectrum has two peaks located at 35.5 and 37.7 eV belonging to W $4f_{7/2}$ and W $4f_{5/2}$, W^{6+} oxidation state, respectively [40]. At the same time, the two peaks around 530.9 and 532.1 eV can be instructed to O 1s, which are communicated to O-Ni bond and lattice oxygen in the $NiWO_4$ phase, respectively [41], all of these proves that $NiWO_4$ exists in ternary compound. Additionally, in the **Fig. 3G**, the Co 2p spectrum exhibits three binding energy at about 777.8 eV, 781.0 eV and 786.1 eV (satellite), which are typical characteristic peaks of CoP [20, 42]. It can be seen from **Fig. 3H**, P 2p spectrum has two peaks, and the peaks locate at 129.2 and 133.3 eV indicate phosphate species due to the surface oxidation [10, 22]. A series of indicators above prove the success load of $NiWO_4$ and CoP on CdS. Comparing to XPS spectra of CSNP-7 before and after hydrogen production, it can be easily found that the valence state and chemical composition of composite catalyst did not change after the reaction.

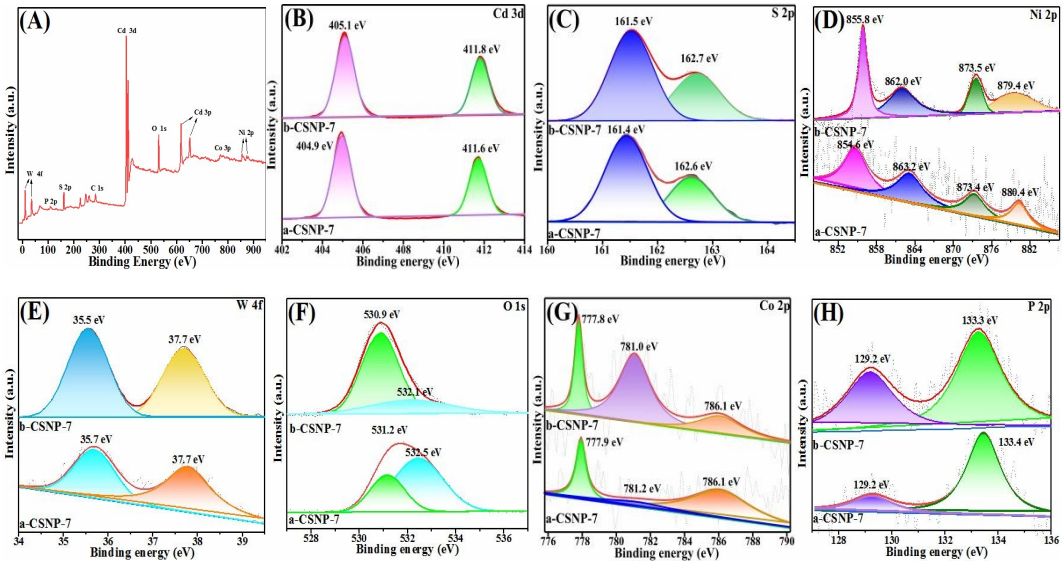

Fig. 3 XPS spectra of **(A)** sample: survey for CSNP-7, **(B)** Cd 3d, **(C)** S 2p, **(D)** Ni 2p, **(E)** W 4f, **(F)** O 1s, **(G)** Co 2p and **(H)** P 2p.

3.4 BET analysis

For purpose of studying the effect of CoP nanoparticles loading on CdS/ $NiWO_4$ catalysts, such as size distribution, specific surface area (S_{BET}) and pore volume are investigated in detail. The nitrogen adsorption and desorption process for CdS, CSNW-5, CSCP-7 and CSNP-7 are performed at 77K. As seen from **Fig. 4A,** the curves for all samples belong to type-IV isotherms, with H3 hysteresis loop [6]. It confirms that all samples have a mesoporous structures, caused by the flock together of nanometer materials [43]. **Fig. 4B** is a schematic diagram of aperture distribution, the pore sizes of four catalysts are concentrated at 2-50 nm and their average pore size is between 18 to 23 nm in **Table 1**, which further proves mesoporous structure of samples. Further analysis of the data was showed in **Table 1**, the S_{BET} of CdS and CSNW are 35.4 and 35.6 $m^2\ g^{-1}$. However, when CoP nanoparticles are supported on two catalysts, the S_{BET} of CSCP and CSNP are 30.2 and 32.4 $m^2\ g^{-1}$, the S_{BET} of composite obviously decreased. Meanwhile pore volume and average bore size of latter is lower than that of former, which probably because some of the pores of CdS are blocked or filled by CoP nanoparticles [21], this conclusion is consistent with the results of TEM and SEM analysis. The changes in performance parameters testify that CoP nanoparticles are successfully loaded onto the surface of the CdS and CSNW-5. Generally speaking, the active sites will increase with the increase of S_{BET}, the S_{BET} of CSCP-7 and CSNP-7 are both increase after adding CoP into the system. Hence, it is demonstrated that the enhanced HER activity of CSNP has nothing to do with the change of S_{BET}.

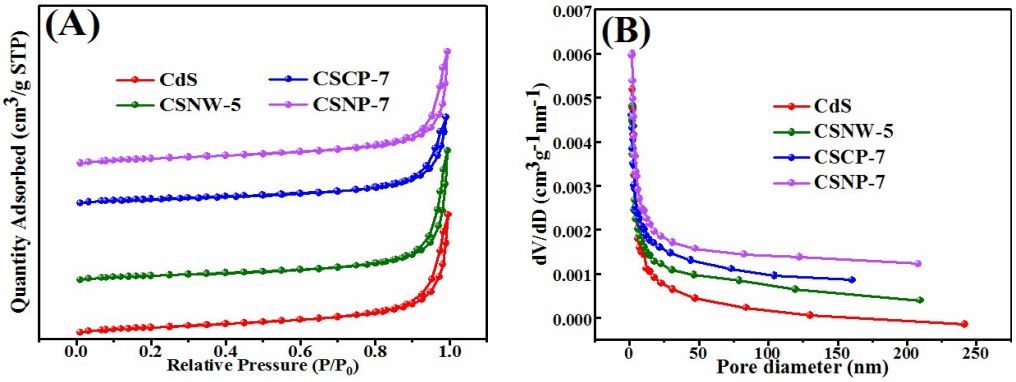

Fig. 4 (A) The N_2 absorption-desorption isotherms and **(B)** corresponding pore size distribution of the all samples.

Table 1 The physical adsorption performance parameters.

Samples	S_{BET} (m^2g^{-1})[a]	Pore volume (cm^3g^{-1})[b]	Average pore size (nm)[b]
CdS	35.4	0.18	21

CSNW-5	35.6	0.20	23
CSCP-7	30.2	0.13	18
CSNP-7	32.4	0.17	22

a Obtained from BET method;

b Relative pressure (P/P0) was 0.99.

3.5 Photocatalytic H_2 evolution performances

Fig. 5 shows the H_2 evolution activities of diverse catalysts with 10% lactic acid solution as a sacrificial agent under visible light irradiation (λ> 400 nm). In **Fig. 5A**, evidently, the pristine $NiWO_4$ has barely any H_2 production activity for 5 h under visible light. At the same time, because CdS is prone to photocorrosion and recombination rate of electron-hole is fast, so H_2 production rate of pure CdS is relatively low. However, hydrogen evolution activity of composite catalyst has been enhanced remarkably due to the addition of $NiWO_4$ and CoP nanoparticles to pure CdS. **Fig. 5B** exhibits the influence of different content the $NiWO_4$ on CSNW activity. With the increase the proportion of $NiWO_4$ loading, the H_2 production rate of CSNW first increase and then decrease. The amount of H_2 production is gradually increased at the beginning, which may attributed to the role of p-n type heterojunction, and then the production of H_2 is decreased because excessive $NiWO_4$ can capture a part of the active sites of CdS [33].

The debugging of CoP nanoparticles is carried out on the optimum ratio of binary catalyst and the results are shown in **Fig. 5C**. The CoP nanoparticles loaded on CSNW-5 can distinctly boost photocatalytic H_2 evolution activity, proving that the CoP nanoparticles are high-efficiency electron trapper. Specially, when the CoP nanoparticle content is 7%, the CSNP-7 composite catalyst shows the highest hydrogen production activity (47.7 mmol h^{-1} g^{-1}). However, the H_2 production began to decrease with the content of CoP nanoparticles increased from 7% to 9%, which may be caused by the shielding effect of the mixed catalyst and the excessive CoP blocking the holes scavengers. In the **Fig. 5D**, the hydrogen production rate over CSNP-7 has 47.4 mmol h^{-1} g^{-1}, which is 11.9 and 3.3 times higher than that of CdS and CSNW-5. In addition, the H_2 evolution rate of CSCP-7 up to 27 mmol h^{-1} g^{-1} under the identical experimental conditions, which is higher than that of CdS and CSNW-5 but far less than that of CSNP-7. In short, a series of comparison experiments prove that the CoP nanoparticles are a co-catalyst with excellent

performance. Further, we provide many H_2 production parameters for the similar potocatalysts, the results are shown in **Table 2**.

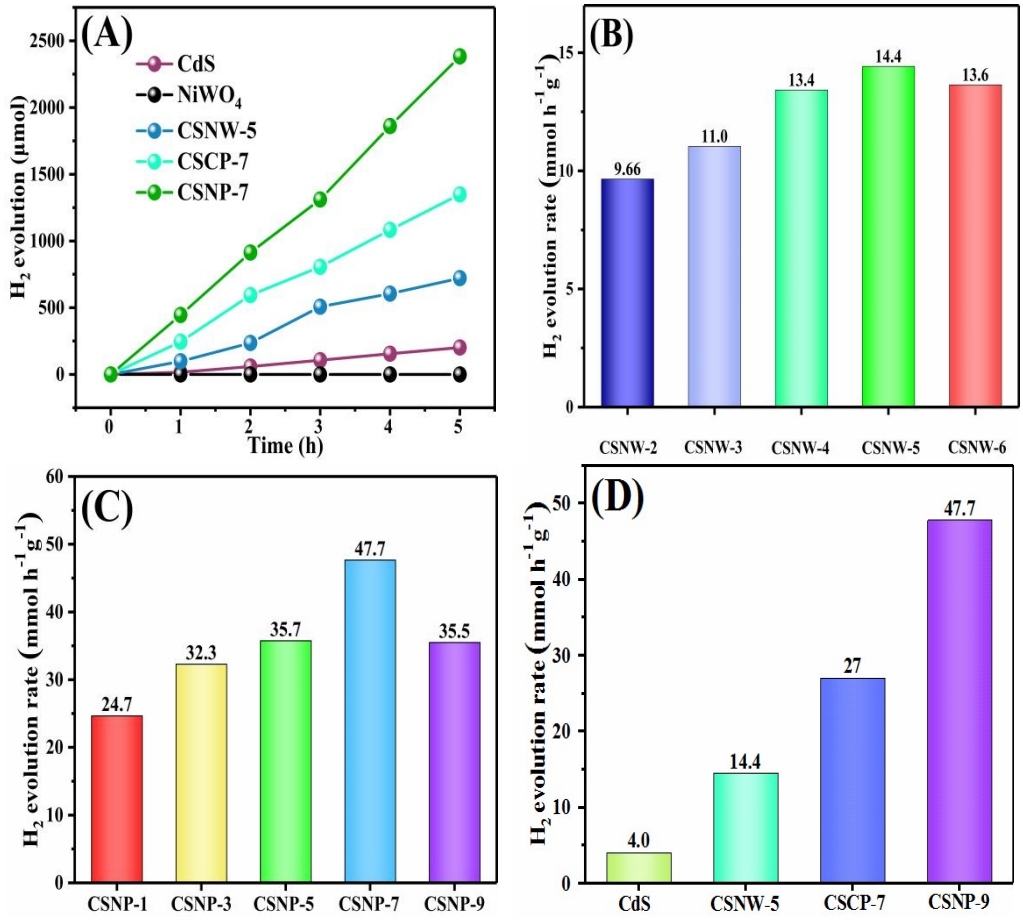

Fig.5 H_2 evolution amount of **(A)** pure CdS, CSNW-5, CSCP-7 and CSNP-7; **(B)** hydrogen production rate of CSNW-X (X=2, 3, 4, 5, 6), **(C)** CSNP-X (X=1, 3, 5, 7, 9) and **(D)** different catalysts.

Besides, hydrogen evolution stability and apparent quantum efficiency (AQE) of CSNP-7 are important indicators to measure the practical application of catalysts. **Fig. 6A** shows three-dimensional diagram of the H_2 production of CSNP-7 in five consecutive circulation of 5 h illumination, after the fifth cycle, the amount of H_2 is accounts for 75% of the first cycle. The reason for this phenomenon may be increased in reaction time, which would further exacerbate consumption of lactic acid. Meanwhile, it also indicates that the CSNP-7 as a kind of composite catalyst shows relatively excellent stability. **Fig. 6B** displays the AQE for CSNP-7 under different incident wavelengths. The AQE value is approximate 8.1%, 5.7%, 9.7%, 4.6%, 0.4% and 0.04% for CSNP-7 at a light source with of 420, 450, 475, 500, 520 and 550 nm, respectively. When the wavelength of the light sources is adjusted to 550 nm, the minimum AQE is only 0.04%,

manifesting that this wavelength is unfavorable to hydrogen generation efficiency of the composite catalyst; the highest AQE of CSNP-7 is 9.7% when the monochromatic wavelength is 475 nm.

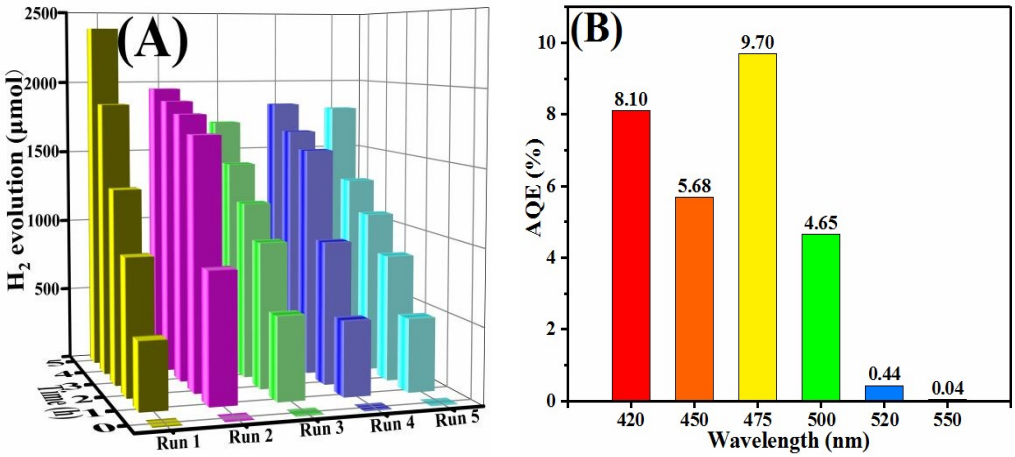

Fig. 6(A) The stability test of hydrogen production cycle of CSNP-7, **(B)** AQE of CSNP-7 in the 420-550 nm wavelength range.

Table 2 Comparison of catalytic activities of other similar photocatalytic decomposition and hydrogen evolution systems

Photocatalyst	Co-catalyst	Light source	Sacrificial reagent	Activity ($\mu mol \cdot h^{-1} \cdot g^{-1}$)	Ref.
CdS	WPS	5 W LED ($\lambda \geq 420nm$)	10 vol% lactic acid	47700	This work
CdS	$NiWO_4$	5 W LED ($\lambda \geq 420nm$)	10 vol% lactic acid	15140	6
Co_3O_4	CoP	400 W Xe-lamp ($\lambda \geq 420nm$)	TEOA (pH=9)	34490	8
$Zn_xCd_{1-x}S$	WP	5 W LED ($\lambda \geq 420nm$)	10 vol% lactic acid	15028	9
CdS	MnO_x@ CoP	300 W Xe-lamp ($\lambda \geq 420nm$)	0.1M Na_2S 0.1M Na_2SO_3	12000	20
g-C_3N_4	NiP	300 W LED ($\lambda \geq 420nm$)	TEOA	362	32
$Zn_{0.7}Cd_{0.3}S$	$NiWO_4$	5W LED ($\lambda \geq 420nm$))	10 vol% lactic acid	15950	38
CdS	Ni_2P	300WXe-lamp ($\lambda \geq 420nm$)	H_2O(artificial gill)	838	40

3.6 Photoluminescence analysis

The PL spectrum of pure CdS, CSNW-5, CSCP-7, CSNP-7 are shown in **Fig. 7A**. Generally

speaking, the intensity of the fluorescent signals and recombination of electrons and holes are considered to be closely related. Emission wavelength of pure CdS is about 520 nm, it shows a relatively strong PL emission intensity, and this indicates that it has a serious recombination rate of electron-hole pairs. The PL intensity of CSNW-5 is lower than that of CdS, the main reason is that CdS and $NiWO_4$ formed p-n type heterojunction, thereby improving the separation effect of electrons and holes [6]. It is interesting to note that PL intensity of CSCP-7 show significant decrease and slight blue shift. It could be because CoP nanoparticles are uniformly distributed character, it can promote electrons transfer by tightly contact with the outer surface of CdS [22], which contributes to control the recombination of electron-hole pairs [47]. The PL intensity of CSNP-7 is the lowest in all the samples due to the CSNP-7 has serious phenomenon of quenching, which indicates that the CSNP-7 has excellent charge separation capacity in photocatalysis system [22]. This excellent performance is attributed to CoP nanoparticles, acting as electron traps to provide more active sites and benefit electron transport. On the other hand, it has the synergistic effects between the CdS, $NiWO_4$ and CoP nanoparticles, which greatly improved the hydrogen performance of composite catalyst. The variation tendency presented by hydrogen production performance of catalysts is well consistent with the photoluminescence, meaning the positive correlation between catalyst performance and degree of charge separation.

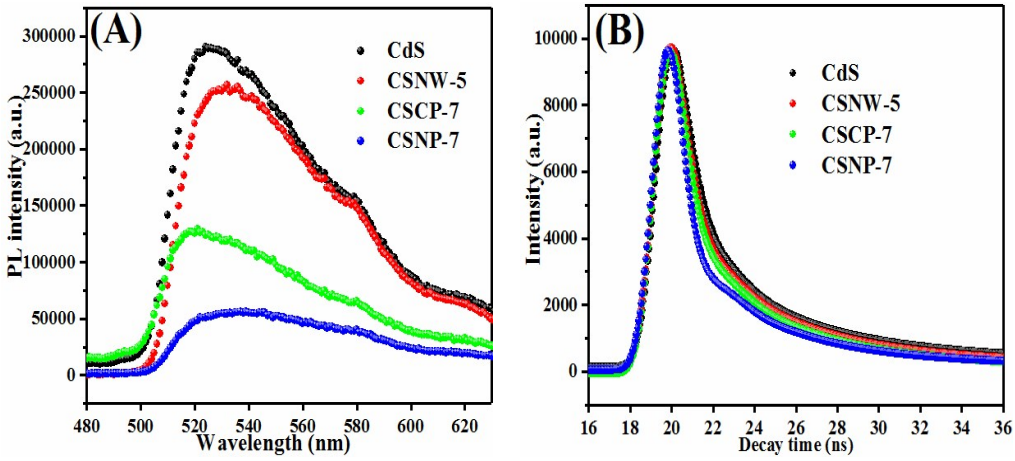

Fig. 7 (A) The PL spectra and **(B)** the time-resolved photoluminescence spectra of CdS, CSNW-5, CSCP-7, CSNP-7.

Fig. 7B displays the kinetics studies of charge transfer coming from the time-resolved photoluminescence (TRPL). The time-resolved photoluminescence of CdS, CSNW-5, CSCP-7

and CSNP-7 samples were tested. The decay curves were achieved by a fitted triexponential decay using the Eq. (2).

$$I(t) = \sum_{i=1,2,3} B_i exp(-t/\tau_i) \quad (2)$$

I is the normalised emission intensity; **t** is the time after the pulsed laser excitation; $\boldsymbol{\tau}_i$ are the respective decay lifetimes; $\mathbf{B}_i$ are the corresponding weight factors.

The average life span of the catalyst is obtained by Eq. (3). **Table 3** shows the dynamics parameters of electron transfer for the samples.

$$\langle \tau \rangle = \sum_{i=1,2,3} B_i \, \tau_i^2 / \sum_{i=1,2,3} B_i \, \tau_i \quad (3)$$

$<\tau>$ is the average lifetime; τ_i is the respective decay times; B_i is the corresponding weight factors.

Usually, electron transfer rate is negatively correlated with the electron lifetime. The average lifetime of CSNP-7 (1.16 ns) is significantly lower than that of CdS (2.27 ns), CSNW-5 (2.23 ns), CSCP-7 (2.19 ns). The results show that CSNP-7 composite material has shorter time of electron transport [46]. This is because CoP can effectively capture the electrons on the outer surface of CdS, which creates additional decay channel to the excited states of the CSNW-5 [21]. In addition, we also analyzed the charge migration of the catalyst by calculating the values of electron transfer rate constant (K_{ET}) and the electron injection efficiency (η_{inj}), they can be calculated by Eq (4) and (5) respectively:

$$K_{ET} = \frac{1}{\tau_{ave}(sample)} - \frac{1}{\tau_{ave}(CS)} \quad (4)$$

$$\eta_{inj} = 1 - \frac{\tau_{ave}(sample)}{\tau_{ave}(CS)} \quad (5)$$

Because of the K_{ET} and η_{inj} value of CSNP-7 are larger than that CSCP-7 and CSNW-5, which manifest that CoP nanoparticles as charge collector can effectively accept electrons attached on the surface of CdS and $NiWO_4$ [21]. Once again, it proves that CoP nanoparticles play a huge role in improving H_2 evolution performance of composite catalyst. When the amount of CoP nanoparticles is 7% to CSNW-5, the photocatalytic performance of composite catalyst is more excellent. On the one hand this is because the CoP as a catalyst exposes more active sites and effectively inhibits the recombine of electrons and holes; On the other hand the synergistic

action of the three substances also has obvious effect on the improvement of catalyst performance.

Table 3 The dynamics parameters of electron transfer for samples.

Samples	τ_1 [ns]	τ_2 [ns]	τ_3 [ns]	τ_{ave} [ns]	K_{ET} [10^9 s^{-1}]	$\eta_{(inj)}$ [%]
CdS	5.47 (27.83%)	0.78 (24.35%)	151.27 (47.81%)	2.72	-	-
CSNW-5	5.10 (28.65%)	0.63 (46.96%)	149.15 (24.39%)	2.23	0.08	18.0
CSCP-7	5.17 (28.82%)	0.63 (24.93%)	147.28 (46.25%)	2.19	0.09	19.5
CSNP-7	4.75 (28.08%)	0.36 (29.13%)	144.04 (42.79%)	1.16	0.49	57.5

3.7 Photoelectrochemical properties

In order to further investigate the electron separation efficiency, electrochemical analyses are executed on the catalysts. In a general way, strength of instantaneous photocurrent response is positively correlated with the separation effect of electrons-holes. **Fig. 8A** shows photocurrent density-time curves of CdS, CSNW-5, CSCP-7 and CSNP-7, the photocurrent is generated when light is irradiated the surface of catalyst, the curves of photocurrent response are accomplished under discontinuous light. From the overall analysis, the photocurrent density of CdS and CSNW-5 remains almost unchanged, CSCP-7 and CSNP-7 shows a decreasing trend with the extension of illumination time. The photocurrent density of CdS is lowest compared, which may be due to photocorrosion. In contrast, the transient photocurrent response of CSNP-7 is higher than the rest of the catalysts, indicating that the CSNP-7 holds stronger ability in generating and transferring the photoexcited charge carrier [8]. This could be because the modification of CoP nanoparticles increases the separation efficiency of photogenerated electrons and holes [23].

In addition, **Fig. 8B** shows the AC impedance spectrum of CdS, CSNW-5, CSCP-7 and CSNP-7 in the absence of light. Compared with other catalysts, CSNP-7 has the smallest arc radius, indicating that it's small charge migrating resistance, and enhanced charge transfer rate [11,

23]. The inset of **Fig. 8B** shows the equivalent circuit diagram, and Rct is an electronic transfer resistor; Rs is the solution resistance. The analysis of EIS and IT together demonstrates that the CoP nanoparticles have greatly improved the electron transfer performance and attested the strengthened effect of it on the segregation [11]. Meanwhile, this result is basically consistent with the hydrogen production activity of the catalyst.

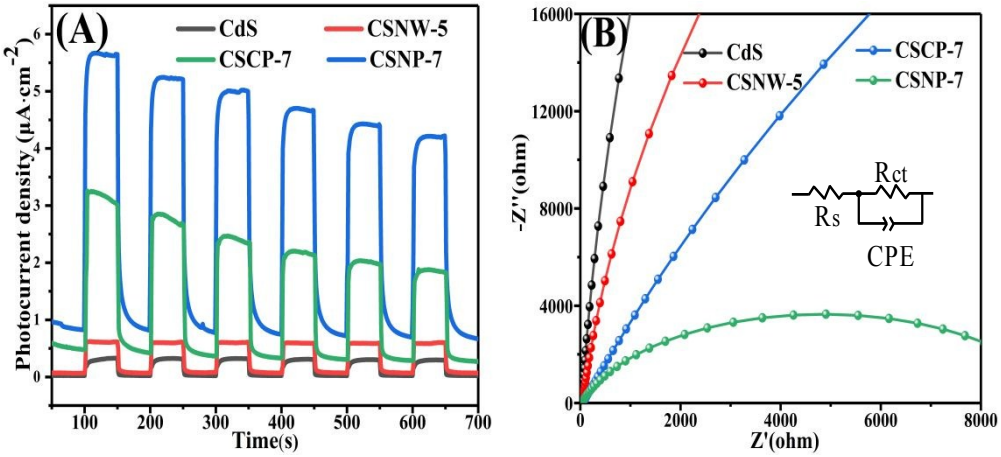

Fig. 8 (A) Transient photocurrent responses of CdS, $NiWO_4$, CSNW-5, CSCP-7 and CSNP-7. **(B)** Electrochemical impedance spectroscopy (EIS) of CdS, $NiWO_4$, CSNW-5, CSCP-7, CSNP-7.

3.8 UV-vis diffuse reflectance spectra and Mott-Schottky analysis

In order to research optical natures of catalysts the UV-vis diffuse reflectance spectra is used to analyze the samples as shown in **Fig. 9A**. Compared with the spectrum of CdS, both the absorption range and the absorption intensity of CSNW-5 have some improvement and the red shift occurs. This is due to a heterostructure was formed between CdS and $NiWO_4$ in the prepared CSNW composites, lending to the redshift of the light absorption of the composite samples [23]. For CSCP-7 and CSNP-7 catalysts, the light absorption range of the composite catalyst was visibly expanded and the light absorption intensity was significantly increased between 510-800 nm. The hydrogen production performance of catalyst was greatly improved. This is because P element has strong light capture ability [23], which expands the absorption range of the catalyst. And by increasing the utilization of sunlight, more photogenerated electron and holes pairs can be generated [48]. On the other hand, the enhancement of light absorption intensity is related to the deepening of catalyst color [6].

The band gap of CdS and $NiWO_4$ samples can be calculated by the following Eq. (6):

View Article Online
DOI: 10.1039/C9NJ05977F

$$\alpha h\upsilon = A(h\upsilon - E_g)^{n/2} \quad (6)$$

α represents absorption coefficient, **h** represents Planck's constant, υ represents light frequency, $\mathbf{E_g}$ represents band-gap energy and A represents a constant, respectively.

Fig. 9B presents energy band gap (E_g) of samples, the E_g of CdS, $NiWO_4$, CSNW-5, CSCP-7 and CSNP-7 are2.33, 2.24, 2.29, 2.23 and 2.18 eV, respectively. All catalysts have E_g less than 3.0 ev, indicating that they are capable of generating photogenerated electrons and holes through photoexcitation. Further analysis finds that the decrease of band gap was due to the addition of CdS nanorods and $NiWO_4$. Catalysts with reduced band gap are more easily excited [48], thereby improving hydrogen production performance of catalysts.

Fig. 9C, D exhibits the Mott-Schottky plots of CdS nanorods and $NiWO_4$. Since CdS nanorods have a positive slope and $NiWO_4$ has a negative slope, CdS nanorods is a characteristic n-type semiconductor and $NiWO_4$ belongs to p-type semiconductor. The flat-band potential (E_{fb}) of CdS and $NiWO_4$ can be computed to be -0.35 and 1.65 V versus. SCE, respectively. On the basis of previous literature, the E_{CB} of n-type semiconductor is more negative 0.1 V or 0.2 V than the E_{fb}; the E_{CB} of p-type semiconductor is more positive about 0.1 V or 0.2 V than its E_{fb}. And then from the formula of Eq: $E_{NHE} = E_{SCE} + 0.24$ V. The E_{CB} of CdS nanorods and E_{VB} of $NiWO_4$ are calculated as -0.31 and 2.09 V versus NHE. According to the formula used to estimate the VB positions of CdS nanorods and CB positions of $NiWO_4$: $E_{CB} = E_{VB} - E_g$. The final calculation results are shown in **Table 4**.

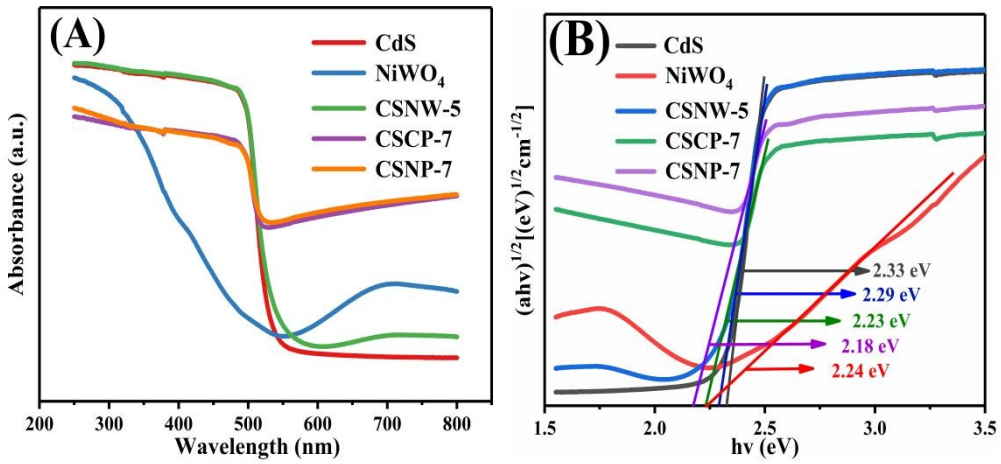

View Article Online
DOI: 10.1039/C9NJ05977F

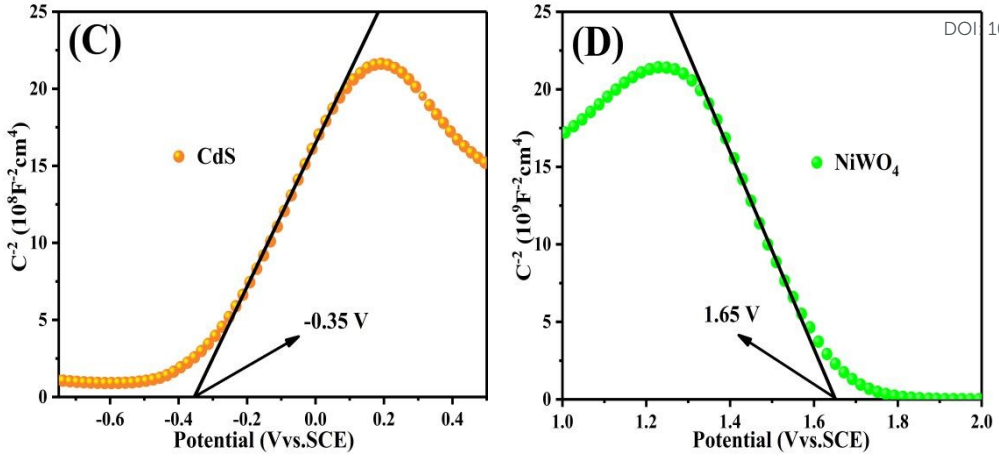

Fig. 9 (A) The UV-vis DRS of CdS, $NiWO_4$, CSNW-5, CSCP-7, CSNP-7; **(B)** The forbidden band width of CdS, $NiWO_4$, CSNW-5, CSCP-7, CSNP-7. Mott-Schottky plots of **(C)** n-type CdS and **(D)** p-type $NiWO_4$.

Table 4 Band gap energy, valence and conduction band edge potential of CdS and $NiWO_4$.

Semiconductor	Band energy E*g* (eV)	Valence band E_{VB} (eV)	Conduction band E_{CB} (eV)
CdS (n-type)	2.30	1.94	-0.31
$NiWO_4$ (p-type)	2.07	2.09	0.02

3.9 Proposed Reaction Mechanism

Firstly, the band gap positions of CdS and NiWO4 are drawn according to **Table 4**. The energy band structure of composite catalyst CSNP-7 before and after touch is shown in **Fig. 10**. Generally, CdS as n-type semiconductor, its Fermi level draw near to CB position. On the contrary, for the p-type semiconductor, Fermi level of $NiWO_4$ is approach to VB position [41]. When CdS nanorods is close contact with $NiWO_4$, because Fermi level of CdS is lower than that $NiWO_4$, which affords a thermodynamic access to speed up charge transfer [6]. The two Fermi levels gradually approach equilibrium. Finally, CdS and $NiWO_4$ form p-n heterojunction and constructs internal electric field from CdS to $NiWO_4$. The CdS and $NiWO_4$ are excited by visible light irradiation to produce electrons and holes, where both electrons move from VB to CB and holes remain in their VB. Because of existence of potential difference and the internal electric field, the electrons of the CB of $NiWO_4$ can be rapidly transferred to CB of CdS, and further shifted to surface of CdS. CoP nanoparticles as a competent electron trapping agent, it can capture and accelerate electron transfer on the surface of CdS. Subsequently, the electron reacts with protons

in the water to form H_2. In the meanwhile, the photogenerated holes on VB of CdS transfer to the VB of $NiWO_4$, the lots of holes assembled on the surface of $NiWO_4$ are expended by lactic acid, while lactic acid is oxidized to produce CO_2 and H_3O^+. In addition, there is also a portion of CoP nanoparticles are adhered onto the surface of $NiWO_4$, part of electron can directly transfer from the CB of $NiWO_4$ to CoP nanoparticles, and then they react with the protons to form H_2. In a word, taking advantage of CoP as a cocatalyst is used to modify CSNW hetero-junction, it can increase separation efficiency of electrons and holes to provide more active sites, and enhance the absorbance of the catalyst, thereby improving of H_2 production activity of the composite catalyst.

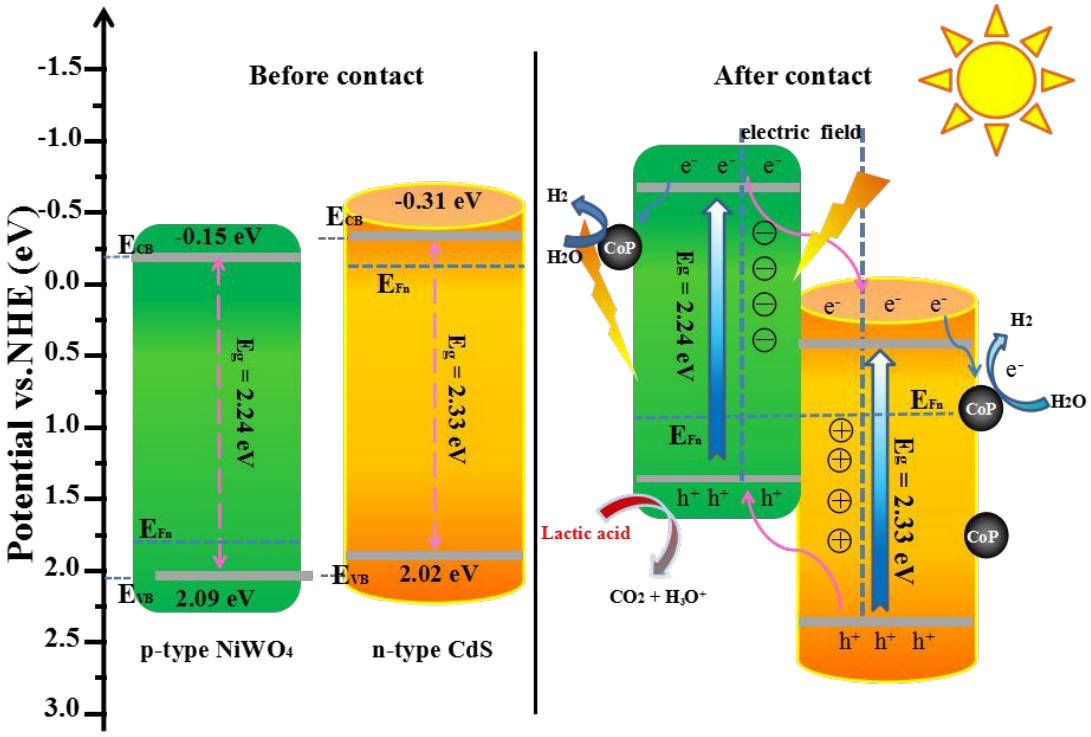

Fig.10 Schematic illustration of charge transfer for CSNP-7

4. Conclusion

In this work, $CdS/NiWO_4$ p-n hetero-junction is successfully modified by CoP nanoparticles. When 10% lactic acid used as a sacrificial agent, the composite catalyst CSNP-7 shows the highest hydrogen production rate (47.7 mmol h^{-1} g^{-1}), which is 11.9 times and 3.3 times that of CdS (4.0 mmol h^{-1} g^{-1}) and CSNW-5 (14.4 mmol h^{-1} g^{-1}). The remarkable improvement in hydrogen production performance can be ascribed to the CoP nanoparticles as an electron trapping agent, it can accelerate the transfer of electrons and provide more active site. In addition, the composite catalyst CSNP-7 has remarkable optical and electrical properties, which have been

investigated by UV-visible diffuse reflectance, test photoluminescence and photoelectrochemical detection. The present study is expected to provide novel insights for using co-catalyst modified the heterojunction to produce hydrogen efficiently.

Author contributions

Hua Liu and Teng Yan conceived and designed the experiments; Hua Liu and Teng Yan performed the experiments; Zhiliang Jin, Qingxiang Ma contributed reagents/materials and analysis tools; and Hua Liu and Teng Yan wrote the paper.

Conflicts of interest

The authors declare that they have no competing interests.

Acknowledgements

This work was financially supported by the Chinese National Natural Science Foundation (21862002, 41663012), the Open Project of State Key Laboratory of High-efficiency Utilization of Coal and Green Chemical Engineering, Ningxia University (2019-KF-36), the new technology and system for clean energy catalytic production, Major scientific project of North Minzu University (ZDZX201803) and the Ningxia low-grade resource high value utilization and environmental chemical integration technology innovation team project of North Minzu University.

Reference:

[1] Xiaoping Tao, Yue Zhao, Luichao Mu, Shengyang Wang, Rengui Li, Bismuth tantalum Oxyhalogen: A promising candidate photocatalyst for solar water splitting, Advanced Energy Material, 2018, 8, 1701392.

[2] Jingxiang Low, Jiaguo Yu, Mietek Jaroniec, Swelm Wageh, Ahmed A. Al-Ghamdi,

Heterojunction photocatalysts, Advanced Materials, 2017, 39, 1601694.

[3] Xuqiang Hao, Yicong Wang, Jun Zhou, Zhiwei Cui, Ying Wang, Zhigang Zou, Zinc vacancy-promoted photocatalytic activity and photostability of ZnS for efficient visible light driven hydrogen evolution, Applied Catalysis B: Environmental. 2018, 221, 302-311.

[4] Quanlong Xu, Liuyang Zhang, Jiaguo Yu, Swelm Wageh, Ahmed A, Al-Ghamdi, Mietek Jaroniec. Direct Z-scheme photocatalysts: principles, synthesis, and applications, Materials Today, 2018, 21, 1042-1063.

[5] D. Praveen Kumar, Sangyeob Hong, D. Amaranatha Reddy, Tae Kyu Kim, Ultrathin MoS2 layers anchored exfoliated reduced graphene oxide nanosheet hybrid as a highly efficient cocatalyst for CdS nanorods towards enhanced photocatalytic hydrogen production, Applied Catalysis B: Environmental, 2017, 212, 7-14.

[6] Yongke Zhang, Zhiliang Jin, Accelerated charge transfer via a nickel tungstate modulated cadmium sulfide p-n heterojunction for photocatalytic hydrogen evolution, Catalysis Science Technology, 2019, 9, 1944-1960.

[7] Junwei Fu, Quanlong Xu, Jingxiang Low, Chuanjia Jiang, Jiaguo Yu, Ultrathin 2D/2D WO_3/g-C_3N_4 step-scheme H_2-production photocatalyst, Applied Catalysis B: Environmental, 2019, 243, 556-565.

[8] Shaoqin Peng, Yang Cao, Fengxian Zhou, Zhaodi Xu, Yuexiang Li, CoP decorated with Co_3O_4 as a cocatalyst for enhanced photocatalytic hydrogen evolution via dye sensitization, Applied Surface Science, 2019, 487, 315-321.

[9] Xian Yan, Zhiliang Jin, Yupeng Zhang, Yongke Zhangaand and Hong Yuan, Sustainable and efficient hydrogen evolution over a noble metal-free WP double modified ZnxCd_{1-x}S photocatalyst driven by visible-light, Dalton Transactions. 2019, 48, 11122-11135.

[10] Xiaoqiang Du, Zhi Yang, Yu Li, Yaqiong Gonga, Min Zhao, Controlled synthesis of $Ni(OH)_2$/Ni_3S_2 hybrid nanosheet arrays as highly active and stable electrocatalysts for water splitting, Journal of Materials Chemistry A, 2018, 16, 6938-6946.

[11] Qiaohong Zhu, Bocheng Qiu, Huan Duan, Yeteng Gong, Zengwei Qin, Bin Shen, Mingyang Xing, Jinlong Zhang, Electron directed migration cooperated with thermodynamic regulation over bimetallic NiFeP/g-C_3N_4 for enhanced photocatalytic hydrogen evolution, Applied Catalysis B: Environmental, 2019, 259, 118078.

[12] Honghui Ou, Chao Tang, Yongfan Zhang, Abdullah M. Asiri, Maria-Magdalena Titirici, Xinchen Wang, Se-modified polymeric carbon nitride nanosheets with improved photocatalytic activities, Journal of Catalysis, 2019, 375, 104-112.

[13] Chenchen Feng, Zhonghao Wang, Ying Ma, Yajun Zhang, Lei Wang, Yingpu Bi, Ultrathin graphitic C_3N_4 nanosheets as highly efficient metal-free cocatalyst for water oxidation. Applied Catalysis B: Environmental, 2017, 205, 19-23.

[14] Chunyang Zhai, Mingjuan Sun, Lixi Zeng,Mianqiang Xue, Jianguo Pan, Yukou Du, Mingjuan Zhu, Construction of Pt/graphitic C_3N_4/MoS_2 heterostructures on photo-enhanced electrocatalytic oxidation of small organic molecules. Applied Catalysis B: Environmental, 2019, 243, 283-293.

[15] Yi Ma, Xiuli Wang, Yushuai Jia, Xiaobo Chen, Hongxian Han, Can Li, Titanium dioxide based banomaterials for photocatalytic fuel generations, Chemical Reviews, 2014, 144, 9987-10043.

[16] Xichen Zhou, Zhen Liu, Yifan Wang, Yong Ding, Facet effect of Co_3O_4 nanocrystals on visible-light driven water oxidation, Applied Catalysis B: Environmental, 2018, 237, 74-84.

[17] Xuqiang Hao, Yicong Wang, Jun Zhou, Zhiwei Cui, Ying Wang, Zhigang Zou, Zinc vacancy-promoted photocatalytic activity and photostability of ZnS for efficient visible light driven hydrogen evolution, Applied Catalysis B: Environmental, 2018, 211, 302-311.

[18] Chao Xue, He Li, Hua An, Bolun Yang, Jinjia Wei, Guidong Yang, NiS_x quantum dots accelerate electron transfer in $Cd_{0.8}Zn_{0.2}S$ photocatalytic system via an rGO nanosheet "Bridge" toward visible-light-driven hydrogen evolution. American Chemical Society, 2018, 8(2), 1532-1545.

[19] Yufei Zhao, Yunxuan Zhao, Geoffrey I. N, Waterhouse, Lirong Zheng, Xingzong Cao, Fei Teng, Li-Zhu Wu, Chen-Ho Tung, Dermot O'Hare, Tierui Zhang, Layered-double-hydroxide nanosheets as efficient visible-light-driven photocatalysts for dinitrogen fixation, Advanced Materials, 2017, 29, 1703828.

[20] Xiaohong Zhang, Nan Li, Jiaojiao Wu, Yanzhen Zheng, Xia Tao, Defect-rich O-incorporated 1T-MoS_2 nanosheets for remarkably enhanced visible-light photocatalytic H_2 evolution over CdS: The impact of enriched defects, Applied Catalysis B: Environmental, 2018, 229, 227-236.

[21] Xiangbin Meng, Jingli Sheng, Hongliang Tang, Xiaojun Sun, Hong Dong, Fengming Zhang, Metal-Organic framework as nanoreactors to Co-incorporate carbon nanodots and CdS quantum dots into the pores for improved H_2 evolution without noble-metal cocatalyst, Applied Catalysis B: Environmental, 2019, 244, 340-346.

[22] Mingyang Xing, Bocheng Qiu, Mengmeng Du, Qiaohong Zhu, Lingzhi Wang, Jinlong Zhang, Spatially separated CdS shells exposed with reduction surfaces for enhancing photocatalytic hydrogen evolution, Advanced Functional Materials, 2017, 27, 1702624.

[23] Zizhong Zhang, Lin Huang, Jiangjie Zhang, Fengjiao Wang, Yanyu Xie, Xiaotong Shang, Yuyao Gu, Huibo Zhao, Xuxu Wang, In situ constructing interfacial contact $MoS_2/ZnIn_2S_4$ heterostructure for enhancing solar photocatalytic hydrogen evolution, Applied Catalysis B: Environmental, 2018, 233, 112-119.

[24] Xuejun Zhou, Hao Yu, Dan Zhao, XinChen Wang, Shoutian Zheng, Combination of polyoxotantalate and metal sulfide: A new-type noble-metal-free binary photocatalyst $Na_8Ta_6O_{19}/Cd_{0.7}Zn_{0.3}S$ for highly efficient visible-light-driven H_2 evolution, Applied Catalysis B: Environmental, 2019, 248, 423-429.

[25] Thomas Simon, Nicolas Bouchonville, Maximilian J. Berr, Aleksandar Vaneski, Asmir Adrovic, David Volbers, Regina Wyrwich, Markus Doblinger, Andrei S. Susha, Andrey L, Rogach, Frank Jackel, Jacek K. Stolarczyk, Jochen Feldmann, Redox shuttle mechanism enhances photocatalytic H_2 generation on Ni-decorated CdS nanorods, Nature Materials, 2014, 13, 1013-1018.

[26] Molly B. Wilker, Katherine E. Shinopoulos, Katherine A. Brown, David W. Mulder, Paul W. King, Gordana Dukovic, Electron transfer kinetics in CdS nanorod-[FeFe]-hydrogenase complexes and implications for photochemical H_2 generation, Journal of the American Chemical Society, 2014, 136, 4316-4324.

[27] Kaifeng Wu, Yongling Du, Hua Tang, Zheyuan Chen, Tianquan Lian, Efficient extraction of trapped holes from colloidal CdS nanorods, Journal of the American Chemical Society, 2015, 137(32), 10224-10230.

[28] Huanli Wang, Lisha Zhang, Zhigang Chen, Junqing Hu, Shijie Li, Zhaohui Wang, Jianshe Liu, Xinchen Wang, Semiconductor heterojunction photocatalysts: design, construction, and photocatalytic performances, Chemical Society Reviews, 2014, 43, 5234-5244.

[29] Mingyang Xing, Bingkun Chen, JiFeng, Wenjing Xu, Yaocai Bai,Yi Zhou, Chunyang Dong, Haizheng Zhong, Jinlong Zhang, Yadong Yin, Confined growth of quantum dots in silica spheres by ion exchange of "Trapped NH4+" for white-light emission, Chem, 2019, 8, 2195-2214.

[30] Yuexiang Li, Hui Li, Yafei Li, Shaoqin Peng, Yunhang Hu, Fe-B alloy coupled with Fe clusters as an efficient cocatalyst for photocatalytic hydrogen evolution, Chemical Engineering Journal, 2018, 344, 506-513.

[31] Guixia Zhao, Yubin Sun, Wei Zhou, Xiangke Wang, Kun Chang, Guigao Liu, Huimin Liu, Tetsuya Kako, and Jinhua Ye, Superior photocatalytic H_2 production with cocatalytic Co/Ni species anchored on sulfide semiconductor, Advanced Materials, 2017, 29, 1703258.

[32] Shuang Cao, Yong Chen, Chuanjun Wang, Xiaojun Lv, Wenfu Fu, Spectacular photocatalytic hydrogen evolution using metal-phosphide/CdS hybrid catalysts under sunlight irradiation, Chemical Communications, 2018, 344, 506-513.

[33] Xiaojing Wang, Xiao Tian, Yingjie Sun, Jiayu Zhu, Fatang Li, Huiying Mu, Jun Zhao, Enhanced schottky effect of a 2D-2D CoP/g-C_3N_4 interface for boosting photocatalytic H_2 evolution, Nanoscale, 2018, 26, 12315-12321.

[34] Yajie Chen, Chuanhong Kang, Ruihong Wang, Zhiyu Ren, Huiying Fu, Yuting Xiao, Guohui Tian, Zijun Sun, Huafei Zheng, Jingshi Li, Pingwu Du, Extraordinarily efficient photocatalytic hydrogen evolution in water using semiconductor nanorods integrated with crystalline Ni_2P cocatalysts, Energy Environmental Science, 2015, 9, 2668-2676.

[35] Wanjun Wang, Taicheng An, Guiying Li, Dehua Xia, Huijun Zhao, Jimmy C, Yu, Po Keung Wong, Earth abundant Ni_2P/g-C_3N_4 lamellar nanohydrids for enhanced photocatalytic hydrogen evolution and bacterial inactivation under visible light irradiation, Applied Catalysis B: Environmental, 2017, 217, 570-580.

[36] Mingjie Li, Shun Yokoyama, Hideyuki Takahashi, Kazuyuki Tohji, Bandgap engineering of $NiWO_4$/CdS solid Z-scheme system via an ionexchange reaction, Applied Catalysis B: Environmental. 2019, 241, 284-291.

[37] Yanbing Li, Zhiliang Jin, Xuqiang Hao, Guorong Wang, Insights into the unique role of cobalt phosphide for boosting hydrogen evolution activity based on MIL-125-NH_2, International Journal of Hydrogen Energy, 2019, 44, 17909-17921.

[38] Razium Ali Soomro, Nazar Hussain Kalwar, Ahmet Avci, Erol Pehlivan, Keith Richard Hallam, Magnus Willander, In-situ growth of $NiWO_4$ saw-blade-like nanostructures and their application in photo-electrochemical (PEC) immunosensor system designed for the detection of neuron-specific enolase, Biosensors and Bioelectronics, 2019, 141, 111331.

[39] Mohamed Mokhtar Mohamed, Saleh A. Ahmed, Khalid S.Khairou, Unprecedented high photocatalytic activity of nanocrystalline $WO_3/NiWO_4$ hetero-junction towards dye degradation: Effect of template and synthesis conditions, Applied Catalysis B: Environmental, 2019, 150, 63-73.

[40] Maria N. Mancheva, Reni S. Iordanova, Dimitar G. Klissurski, Georgi T. Tyuliev, Boris N. Kune, Direct Mechanochemical Synthesis of Nanocrystalline $NiWO_4$. The Journal of Chemical Physics, 2007, 111, 1101-1104.

[41] Yang Liu, Guorong Wang, Yanbing Li, Zhiliang Jin, 2D/1D $Zn_{0.7}Cd_{0.3}S$ p-n heterogeneous junction enhanced with $NiWO_4$ for efficient photocatalytic hydrogen evolution, ournal of Colloid and Interface Science, 2019, 554, 113-124.

[42] Xiaoqiang Du, Hui Su, Xiaoshuang Zhang, Metal organic framework derived Cu-doped Co_9S_8 nanorod array with less low-valence Co sites as highly efficient bifunctional electrodes for overall water splitting, ACS Sustainable Chemistry Engineering, 2019, 19, 16917-16926.

[43] D. Praveen Kumar, Sangyeob Hong, D. Amaranatha Reddy, Tae Kyu Kim, Ultrathin MoS_2 layers anchored exfoliated reduced graphene oxide nanosheet hybrid as a highly efficient cocatalyst for CdS nanorods towards enhanced photocatalytic hydrogen production, Applied Catalysis B: Environmental, 2017, 212, 7-14.

[44] Wenlong Zhen, Xiaofeng Ning, Baojun Yang, Yuqi Wu, Zhen Li, Gongxuan Lu, The enhancement of CdS photocatalytic activity for water splitting via anti-photocorrosion by coating Ni_2P shell and removing nascent formed oxygen with artificial gill, Applied Catalysis B: Environmental, 2018, 221, 243-257.

[45] Ruya Cao, Hongcen Yang, Shouwei Zhang, Xijin Xu, Engineering of Z-scheme 2D/3D architectures with $Ni(OH)_2$ on 3D porous g-C_3N_4 for efficiently photocatalytic H_2 evolution, Applied Catalysis B: Environmental, 2019, 258, 117997.

[46] Qunzeng Huang, Zejuan Tao, Liqun Ye, Hongchang Yao, Zhongjun Li, $Mn_{0.2}Cd_{0.8}S$ nanowires modified by CoP_3 nanoparticles for highly efficient photocatalytic H_2 evolution

under visible light irradiation, Applied Catalysis B: Environmental, 2018, 237, 689-698.

[47] Zizheng Ai, Yongliang Shao, Bin Chang, Lei Zhang, Jianxing Shen, Yongzhong Wu, Baibiao Huang, Xiaopeng Hao, Rational modulation of p-n homojunction in P-doped g-C_3N_4 decorated with Ti_3C_2 for photocatalytic overall water splitting, Applied Catalysis B: Environmental, 2019, 259, 118077.